J. Fluid Mech. (1986), *vol.* 166, *pp.* 21–39
Printed in Great Britain

Convection in horizontal cavities

By P. G. SIMPKINS AND K. S. CHEN†
AT&T Bell Laboratories, Murray Hill, New Jersey 07974

(Received 8 July 1985)

Flows in water-filled rectangular cavities due to an applied horizontal temperature gradient are examined for Rayleigh numbers, based on height, $R \geqslant 10^6$ and aspect ratios (length/height) $L \geqslant 2$. Laser Doppler velocimetry measurements of the horizontal velocity distribution throughout the core are complemented with local temperature measurements and interferometry observations. The results show that the core stream function is aspect-ratio dependent when $R > O(10^5)$ and the Prandtl number is fixed. When $R \leqslant 10^6$ it appears that the layers on the horizontal surfaces fill the cavity depth if $L \geqslant 3$. For values of $R \geqslant 10^7$ and $L = 2$ the motion in the core is extremely small and the mass flux occurs in layers adjacent to the horizontal walls. Computations of the heat transfer across the cavity are in good agreement with numerical solutions of the vertical boundary-layer equations.

1. Introduction

Thermally driven convective motions due to temperature gradients that are not aligned with gravity occur in numerous situations that are of interest to scientists in a variety of disciplines. Depending on the magnitude of certain parameters the applications include the heat transfer across thermopane windows, the spreading of smoke from fires in buildings, the cooling of nuclear reactors and the preparation of semi-conductor materials from the melt. Some geophysical and meteorological phenomena may also be modelled by such flow systems. The simplest realistic model for flows of this type is an enclosed two-dimensional rectangular cavity with differentially heated vertical end walls. Both horizontal surfaces are usually considered to be rigid and adiabatic, although recently some work has been done with rigid, perfectly conducting surfaces. From both the experimental and the analytical point of view the model is attractive, since it enables the experiment to be well controlled, and the symmetrical boundary conditions reduce the mathematical complexity. Useful summaries of earlier work on the subject have been given by Batchelor (1954), Ostrach (1972) and Catton (1978); consequently, only a few works which deal with particular situations will be mentioned here.

The controlling parameters in the two-dimensional situation are the Rayleigh number R, the Prandtl number σ, and the aspect ratio L (length/height). For many applications R, based on the cavity height, is large and the motion involves thin shear layers near the vertical surfaces. Descriptions of the flow-field structure in the core region, compatible with boundary layers on the end walls, have been given by Singh & Cowling (1963) for the magneto-hydrodynamic case and by Gill (1966) for a Newtonian fluid. These studies of the boundary-layer regime, $R \to \infty$, L fixed, demonstrated that for $\sigma > 1$ the core was vertically stratified, consistent with the

† Current address: Department of Mechanical Engineering, National Sun Yat-Sen University, Kaohsiung, Taiwan.

experimental observations by Eckert & Carlson (1961) and by Elder (1965). None of the early experimental studies considered the flow near the horizontal surfaces and, in order to complete the analytical description, Gill had to assume the horizontal boundary layers were vanishingly small. Interest in the case when $L > 1$ has only developed recently with the realization that, for a given value of σ, a variety of steady-state structures could occur depending on the relative magnitudes of R and L. At the two extremes, when $L \to \infty$ with R fixed and $R \to \infty$ with L fixed, the core flow is parallel to the horizontal boundaries, but other important features of the flow field are quite different. The limit ($L \to \infty$, R fixed) originally examined by Hadley (1735) consists of a diffusion dominated core with dynamically passive, approximately square, end regions in which the flow turns through 180°. This limit has been studied by Cormack, Leal & Imberger (1974) and more recently by Hart (1983*a*). In contrast to the Hadley regime, the boundary-layer limit ($R \to \infty$, L fixed) has a core flow which is stably stratified and diffusion is only important near the boundaries. Most of the temperature drop across the cavity in this case takes place near the end walls. There, the motion generated by large horizontal temperature gradients dominates the flow and provides the driving force for the overall circulation (see Gill 1966).

The flow field evolution between the two limiting situations described above is not well understood. Particular situations have been considered numerically (see, for example, Quon 1977 and Vahl Davis & Jones 1982) but in general a coherent picture of the development has yet to be described. A number of approximate models, in which a selected core-flow behaviour is connected to a boundary layer on the vertical end walls, have also been proposed. The earliest of these models was given by Bejan & Tien (1978), who suggested that in the boundary-layer regime a Hadley cell core could be coupled to the end-wall boundary layers. This procedure led to a qualitative expression for the heat transfer across the cavity, but it must be emphasized that a detailed description of the flow field was not used to achieve the result. Rather, simple connection requirements imposed at the cavity mid-height on the velocity and temperature fields enabled certain unknowns to be evaluated. Since it is known that the Hadley limit, and perturbations due to increasing Rayleigh number, do not admit boundary-layer end-wall regions (see Cormack *et al.* 1974 and Hart 1983*b*), the model must be regarded as an approximation for the heat transfer. Shiralkar, Gadgil & Tien (1981) introduced an outer flow characterized by boundary layers on the horizontal surfaces and a stagnant stratified core. Again connection to vertical end-wall boundary layers was made by matching at the mid-height, a procedure which does not reveal details of the corner flows. A modification of the above method was used by Tichy & Gadgil (1982) with the object of obtaining details of the flow field. Because of difficulties near the corner regions, however, and with matching to the core, a number of simplifying assumptions were introduced. In particular, the horizontal boundary layers were assumed to be of constant thickness, thus implying that the core flow is parallel to the horizontal surfaces. Experimental observations in the large-Rayleigh-number, finite-aspect-ratio regime are often at odds with such an assumption.

Some experimental observations for $L > 1$ have recently been reported, but the amount of detailed information is limited. Bejan, Al-Homoud & Imberger (1981) described some high-Rayleigh-number measurements in a cavity of aspect ratio $L = 16$. Their results with water indicate that the core flow is not parallel to the horizontal surfaces and that it is dominated by intrusion jets near these surfaces. Estimates of the core shear profiles were made by tracking the dye streaks from potassium permanganate pellets dropped into the cavity. Simpkins & Dudderar

(1981) measured the core shear profiles in cavities with aspect ratios $L \leqslant 9$ and found that the core stream function is strongly L-dependent when $R > 10^4$. These results suggested that, in the regime under examination, the horizontal boundary layers significantly affect the core flow field. Measurements of the heat transfer across water-filled cavities with $L = 5$ and with $L = 16$ have been given by Kamotani, Wang & Ostrach (1983). Detailed velocity distributions using laser-Doppler velocimetry have been reported recently by Kirdyashkin (1984) for a rectangular geometry, and by Schiroky & Rosenberger (1984) for a horizontal cylindrical geometry. Both of these works confirm that the shear layers adjacent to the horizontal surfaces are often a significant fraction of the cavity height and therefore, the diffusive effects are important.

When the horizontal surfaces are conducting rather than insulated, thermal oscillations can occur in the flow. Briggs & Jones (1982, private communication) have observed such oscillations in a unit aspect ratio, water-filled cavity, and also noted that the periodicity did not persist under the same thermal conditions when the horizontal surfaces were made adiabatic. Numerical computations qualitatively support these observations and confirm that centro-symmetric behaviour persists even in the periodic state. Hart (1972) showed that, for the Hadley cell, the thermal field is statically unstable when the horizontal surfaces are conductive because the local vertical temperature gradient is negative. In this situation the transverse modes are the most unstable but derive their energy from different sources depending on the value of the Prandtl number. All of the work reported below is for insulated horizontal boundaries and the matter of conducting walls will not be considered further.

Some of the results presented in this paper have been reported briefly at a NATO Advanced Study Institute on Natural Convection (see Simpkins & Chen 1985).

2. Models and appropriate scaling laws

Subject to the Boussinesq approximation the governing equations for the flow in a rectangular cavity with differentially heated end walls are

$$\frac{\partial(\nabla^2\bar{\psi}, \bar{\psi})}{\partial(\bar{x}, \bar{z})} = \sigma\nabla^4\bar{\psi} - \sigma R\frac{\partial\bar{T}}{\partial\bar{x}}, \tag{1}$$

and

$$\frac{\partial(\bar{T}, \bar{\psi})}{\partial(\bar{x}, \bar{z})} = \nabla^2\bar{T}. \tag{2}$$

In the above expressions $\bar{T}$ is the temperature measured from the left-hand cold wall at $\bar{x} = 0$, and it is made dimensionless by the temperature difference T_w^* acting across the cavity. The stream function $\bar{\psi}$ is non-dimensionalized with respect to the thermal diffusivity κ^*. Distances are made dimensionless with respect to h^* the cavity height, and are defined by a Cartesian coordinate system $(\bar{x}, \bar{z})$ whose origin is at the lower corner of the cold wall. Also in (1)

$$R = \frac{g^*\beta^*T_w^*h^{*3}}{\nu^*\kappa^*}, \tag{3}$$

is the Rayleigh number and

$$\sigma = \frac{\nu^*}{\kappa^*} \tag{4}$$

is the Prandtl number, where g^* is the acceleration due to gravity, β^* is the coefficient of thermal expansion and ν^* is the kinematic viscosity.

Appropriate boundary conditions on the vertical end walls are

$$\left.\begin{aligned} \bar{\psi} = \frac{\partial \bar{\psi}}{\partial \bar{x}} = \bar{T} = 0 \quad (\bar{x} = 0), \\ \bar{\psi} = \frac{\partial \bar{\psi}}{\partial \bar{x}} = 0, \bar{T} = 1 \quad (\bar{x} = L), \end{aligned}\right\} \tag{5}$$

where L is the cavity aspect ratio. It is assumed that the horizontal boundaries are adiabatic in all that follows, so that

$$\bar{\psi} = \frac{\partial \bar{\psi}}{\partial \bar{z}} = \frac{\partial \bar{T}}{\partial \bar{z}} = 0 \quad (\bar{z} = 0, 1). \tag{6}$$

As noted by Gill (1966), the above equations and boundary conditions possess the following centro-symmetry properties

$$\left.\begin{aligned} \bar{\psi}(\bar{x}, \bar{z}) = \bar{\psi}(L - \bar{x}, 1 - \bar{z}), \\ \bar{T}(\bar{x}, \bar{z}) = 1 - \bar{T}(L - \bar{x}, 1 - \bar{z}). \end{aligned}\right\} \tag{7}$$

2.1. *Hadley limit – R fixed, $L \to \infty$*

This limiting behaviour has been studied by Cormack, Leal & Imberger (1974) and by Hart (1972, 1983*a*, *b*). Following the arguments of Cormack *et al.*, the characteristic length scale for the core in the $\bar{x}$-direction is $O(L)$; thus the coordinates are scaled

$$X = \frac{\bar{x}}{L}, \quad z = \bar{z}. \tag{8}$$

For a constant longitudinal temperature gradient, the vorticity and energy equations in the core possess an exact parallel flow solution. When centro-symmetry is satisfied, the solution is given by

$$\bar{\psi} = \frac{RC}{24L} z^2 (1 - z)^2, \tag{9a}$$

or

$$\bar{u} = \frac{\partial \bar{\psi}}{\partial z} = \frac{RC}{12L} z(1 - z)(1 - 2z), \tag{9b}$$

and

$$\bar{T} = CX + \frac{RC^2}{24L^2} \left\{ \frac{z^5}{5} - \frac{z^4}{2} + \frac{z^3}{3} \right\} + \tfrac{1}{2}(1 - C) + \left(\frac{RC^2}{1440L^2} \right). \tag{10}$$

Thus, the core consists of a parallel shear flow, with a simple cubic velocity profile, which is driven by a horizontal temperature gradient. Diffusion is the dominant mechanism in the core, and heat is transferred across the cavity primarily by conduction. Figure 1 shows, schematically, the temperature distribution across the core and its derivatives. As noted by Hart (1983*b*), vertical variations in $\bar{T}$ are everywhere statically stable.

The constant C can be written as a regular expansion in inverse powers of L whose coefficients are found by matching with the solution in the end region of the cavity as $X \to 0$. Near each end of the cavity the flow must turn through 180° to satisfy the zero mass flux conditions on the end walls. These regions are approximately square and, in contrast to the boundary-layer limit, dynamically passive. Since the velocity field in the core is parallel to all orders in L^{-1} this structure necessitates that *all* streamlines eventually enter the end region. Furthermore, the scaling used for the

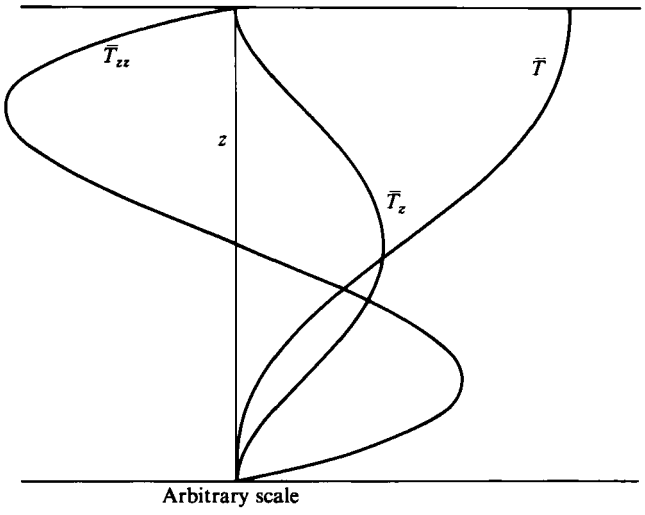

FIGURE 1. Thermal field in a Hadley cell.

horizontal velocity in the core must be maintained in the analysis of the end region, which has characteristic length scales of $O(h^*)$. Hence (1) and (2) must be solved subject to (6), (7) and the matching conditions as $x = \bar{x} \to \infty$. This procedure has been carried out by Cormack *et al.* (1974) for $R = O(1)$ and by Hart (1983*b*) for $R = O(L)$. The approaches for the core structure are essentially similar; the different orders chosen for R lead to a re-ordering of the terms in the expansions. Note, however, that the end structures for the two approaches are very different. Numerical solutions by Cormack *et al.* (1974) for the Hadley regime show that as $L \to \infty$,

$$C \sim 1 - 3.48 \times 10^{-6}\, R^2/L^3; \tag{11a}$$

to this order C is independent of σ. Prandtl number effects arise from the end layers, and in the limit considered by Hart (1983*b*), (11*a*) is replaced by

$$C = 1 + L^{-1} F\left\{\frac{R}{L}, \sigma\right\} + \ldots . \tag{11b}$$

Hart found that for σ sufficiently small the associated end-layer structure does not even permit a parallel flow core.

2.2. *Boundary layer limit* – $R \to \infty$, L *fixed*

Analytical studies of this limit have been reported by Gill (1966), Blythe & Simpkins (1977), and Blythe, Daniels & Simpkins (1983). When the Rayleigh number is large, diffusive effects are confined to thin viscous and thermal layers near the cavity walls. Adjacent to the vertical end walls a balance occurs between convection, viscous and buoyancy effects. The structure of a boundary layer of this type is well known (see Squire 1953 and Gill 1966), and it has a thickness $O(R^{-\frac{1}{4}})$. Suitable independent variables for the vertical boundary layer on the cold wall are

$$\bar{x} = R^{-\frac{1}{4}} \hat{x}, \quad \bar{z} = \hat{z}, \tag{12}$$

and the dependent variables have local expansions of the form

$$\bar{\psi}(\bar{x}, \bar{z}; R, \sigma) = R^{\frac{1}{4}} \hat{\psi}(\hat{x}, \hat{z}; \sigma) + \ldots, \quad \bar{T}(\bar{x}, \bar{z}; R, \sigma) = \hat{T}(\hat{x}, \hat{z}; \sigma) + \ldots . \tag{13}$$

Consistent with (13), the corresponding core structure implies that the flow is vertically stratified, with

$$T_c = \hat{T}_\infty(\hat{z};\sigma), \quad \psi_c = \hat{\psi}_\infty(\hat{z};\sigma). \tag{14}$$

At this stage the core variables $\hat{T}_\infty$ and $\hat{\psi}_\infty$ are unknown and must, in general, be determined from the solutions of both the vertical and the horizontal boundary-layer equations. Unfortunately the structure of the horizontal layers has not yet been found. However, for the singular limit $\sigma \to \infty$, applied subsequently to the formal boundary-layer scaling, Gill (1966) developed a core solution from the vertical boundary-layer equations alone, based on an Oseen approximation. This solution utilized the supplementary condition that all of the mass in the vertical boundary layers emptied into core, i.e. that the horizontal layers, whatever their structure, are negligibly thin.

Another approximate solution, based on an integral technique, has been given by Blythe & Simpkins (1977). This non-linear solution utilized Gill's mass flux hypothesis, but gave results in better accord with numerical computations than the linearized Oseen approximation. One particular result from the integral solution is useful for the present discussion. After a convenient transformation of the dependent variables, the core temperature gradient can be expressed as

$$\frac{\mathrm{d}z}{\mathrm{d}T_\infty} = (1-a)\,(2\psi_m)^{\frac{4}{3}}\,\phi(T_\infty;a), \tag{15}$$

where

$$\phi(T_\infty, a) = [4T_\infty(1-T_\infty)]^{\frac{4-7a}{3a}}\left[\left(\frac{T_\infty}{4}\right)^{\frac{1}{3}} + \left(\frac{1-T_\infty}{4}\right)^{\frac{1}{3}}\right]^{\frac{3a-4}{a}}. \tag{16}$$

Note that in (15) $\psi_m = \psi_\infty(\frac{1}{2})$, and the results satisfy the centro-symmetry relations (7) which, in the core, become

$$\hat{\psi}_\infty(z) = \hat{\psi}_\infty(1-\hat{z}), \quad \hat{T}_\infty(\hat{z}) = 1-\hat{T}_\infty(1-\hat{z}). \tag{17}$$

The choice of the constant a in (15) depends on the form of the profile selected; a good choice is $a = \frac{1}{4}$.

Schematics of the core temperature distribution and its first two derivatives are given in figure 2. Portions of the curves near $z = (0, 1)$, shown as chain-dotted lines, are anticipated adjustments which must occur across the horizontal boundary layers to comply with the imposed boundary conditions. These adjustments are not considered in the approximate methods, where the mass-flux hypothesis is sufficient to complete the solution.

There are noticeable differences between the boundary-layer model of the core temperature field and the Hadley model of the same. Although the core flow is parallel to the horizontal surfaces in both cases, in the present limit the flow is stratified but non-diffusive. This result implies that most of the temperature drop across the cavity takes place near the end walls. It is the vorticity generated in these regions, by the large horizontal temperature gradients, that dominates the flow and provides the driving force for the overall circulation. Motion in the core occurs only as a result of the entrainment and detrainment of mass via the vertical boundary layers (Gill 1966). Diffusive effects are only important near the boundaries and the motion in the core essentially plays a passive role. If this is the case, then, as illustrated in figure 2, the stationary value of the core temperature gradient will be locally a minimum. Such a conclusion contrasts with the Hadley core where $(\mathrm{d}T/\mathrm{d}z)_{\frac{1}{2}}$ is a maximum, see figure 1. The latter situation could only be achieved when $R \gg 1$ if the layers near

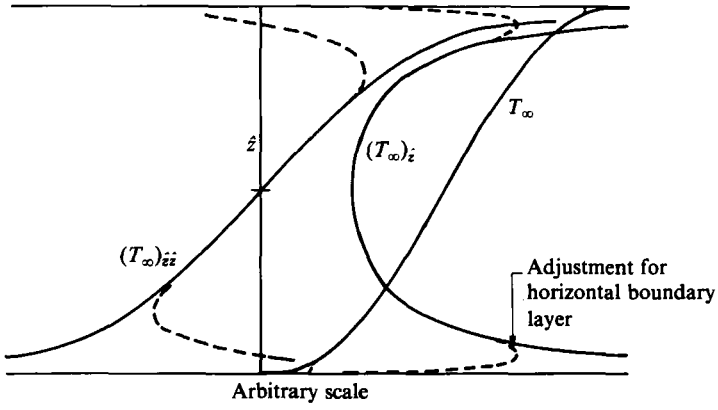

FIGURE 2. Thermal field in the boundary-layer model.

the horizontal surfaces diffuse throughout the core and merge together. Another manifestation of the differences between the temperature gradient profiles in the two limits is that sgn (d^2T/dz^2) changes.

It is important to note that the boundary-layer model is not only valid for $L < 1$. For $L > 1$ the core structure is the same, but as noted earlier, layers adjacent to the horizontal surfaces eventually become large enough to make their presence felt, and ultimately they can fill the cavity. When this merged layer regime occurs, neither the boundary-layer description, nor the parallel-flow Hadley cell is appropriate. A different solution structure in which diffusive effects are taken into account across the core flow must then be developed.

3. Experimental methods

Various techniques have been used to examine the convective flows in cavities with $2 \leqslant L \leqslant 5$. Water was used as the test medium because of its suitability for non-invasive measurements and because the refractive index dependence on temperature is accurately known. The experimental arrangement is a modified design of one used earlier by Simpkins & Dudderar (1981). Quartz glass plate 4.8 mm (0.188 in) thick is used for the vertical sides of a channel which is 560 mm (22.5 in) long, 108 mm (4.30 in) high and 51.6 mm (2.03 in) broad. Two sheets of similar quartz glass form the bottom of the channel which is supported externally by an additional sheet of 12 mm (0.5 in) Plexiglas. Inside the channel two copper thermodes form the vertical end walls which can be adjusted longitudinally, to alter the cavity length. These thermodes are insulated on the top with polystyrene foam, and on the rear surface with a composite layer of asbestos and Teflon; the side walls are separated from the quartz channel by a narrow gap (about 0.25 mm).

Constant-temperature water, or methanol, is pumped from thermostatically controlled circulators to each of the thermodes, thus enabling a temperature difference to be generated across the cavity. Locally, the inlet and outlet temperatures, and the front surface temperature of each thermode is measured with copper–constantan thermocouples. Heat losses to the atmosphere are reduced by operating the circulators at temperatures equally above and below the ambient. During the experiments the laboratory temperature may vary by about ± 1 °C over the, approximately three-hour, period in which the data are recorded. Prior to the

measurements the apparatus has been in operation typically for about 4 h, which is about eight times the characteristic spin-up time $O(h^*l^*/\nu^* R^{\frac{1}{2}})$. Surrounding the quartz chamber is a Plexiglas support structure which can be filled with additional polystyrene foam insulation. The support structure is mounted on jacks which enable the entire assembly to be moved vertically about ± 4 cms relative to the plane of the laser Doppler velocimeter (LDV).

3.1. *The LDV system*

Local velocity measurements are made with a one-component LDV system operating in a forward-scattering, dual-beam mode. The principal components used in the system are a 35 mW helium–neon laser (Spectra-Physics), a high quantum efficiency, low dark current extended S-20 photo-detector (EMI 9658R) and an autodyne frequency tracker (Communications and Electronics); see Wilmshurst & Rizzo (1974). A 400 mm focal length achromat forms the probe volume which has a waist diameter of approximately 0.25 mm. Within the probe volume there are about forty-five fringes between the e^{-2} points, with a spacing of approximately 5.2 μm. Directional velocity discrimination is achieved by frequency shifting both beams of the input signal. Differentially mixing the input signal from each of these two acousto-optic modulators superimposes a 50 kHz frequency on the fringe field. Calibration of the system is performed before and after each test by comparing the output recorded from a stationary scatterer, with that obtained directly from the differential signal of the acousto-optic modulators. These calibrations are typically in agreement to within ± 5 Hz, which corresponds to a velocity of ± 25 μm/s. A minimum of five hundred frequency samples are usually recorded for each measurement which is calculated from the ensemble average. Resolution of these data is believed to be accurate to 50 μm/s.

It should be emphasized that the interest here is strictly in the two-dimensional flow field. For large R the relevant length scale in the third dimension is the sidewall boundary larger thickness δ^*. Provided $\delta^*/b^* \ll 1$, where b^* is the breadth, the motion far from the wall is expected to be two-dimensional. Figure 3 shows a set of data taken about 1 cm apart spanwise to confirm the two-dimensionality of the core region. All other LDV measurements reported herein are from the cavity centre-plane to ensure minimal bias from the sidewalls.

The optical components used to form the probe volume and to collect the transmitted signal, together with the photo-detector, are all mounted on a rigid optical rail. Carriages mounted on twin-rail assemblies that are perpendicular to the optical path enable the LDV probe to be traversed over a distance of 30 cm and positioned to within an accuracy of 25 μm. Extraneous vibrations are minimized by installing the entire experimental arrangement on a pneumatically isolated optical table.

3.2. *Thermal instrumentation*

Local temperature measurements within the cavity are recorded at various distances from the endwalls with a chromel–alumel thermocouple probe made from 0.125 mm wire. The probe is mounted on an electro-mechanical traversing assembly which is driven by a synchronous motor. Observations of the probe output are recorded with a digital temperature sensor and a digital voltmeter. Prior to recording the temperature distributions the instrumentation was calibrated by the ice bath method of establishing a zero reference point and adjusting a one microvolt resolution e.m.f. supply directly to the NBS thermocouple table, thus eliminating the need for ambient compensation.

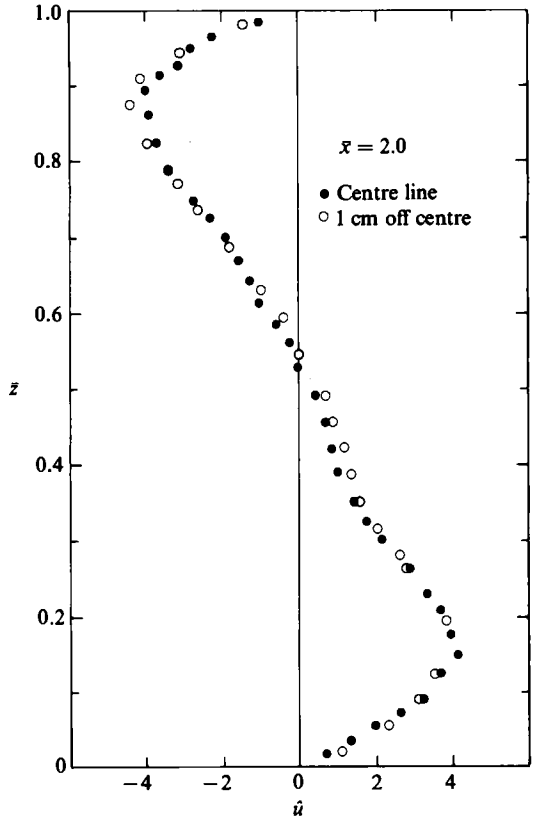

FIGURE 3. Flow field two-dimensionality; $R = 1.3 \times 10^6$, $L = 4$.

Each measurement therefore has an accuracy of about 0.5% and is taken to 0.1 °C resolution.

Observations were also made of the convective flow field using a shearing interferometer similar to that described by Merzkirch (1974) and by Bryngdahl (1965). A collimated 10 cm diameter HeNe laser beam was passed through the cell and onto a parallel sided holographic quality glass plate, which acts as the shearing element. When the incident beam passes through a region in which the refractive index varies, the interference fringes, which represent regions of constant density gradient, are distorted in the recording plane. The direction of the gradient is determined by the orientation of the shearing element relative to the incident beam. This method records regions of constant temperature gradient to an accuracy of about 0.03 °C mm^{-1} per fringe when the shearing element is inclined at 45° to the incident beam.

4. Experimental results

4.1. *Velocity measurements*

Measurements of the horizontal velocity component across the cavity height at different $\bar{x}$ locations were made with R and L as the parameters. Figures 4, 5 and 6 show the velocity distributions measured in cavities with $L = 2$ and 4, at $R \approx 10^6$ and 10^7. Comparison of these three results suggests that the motion illustrated in

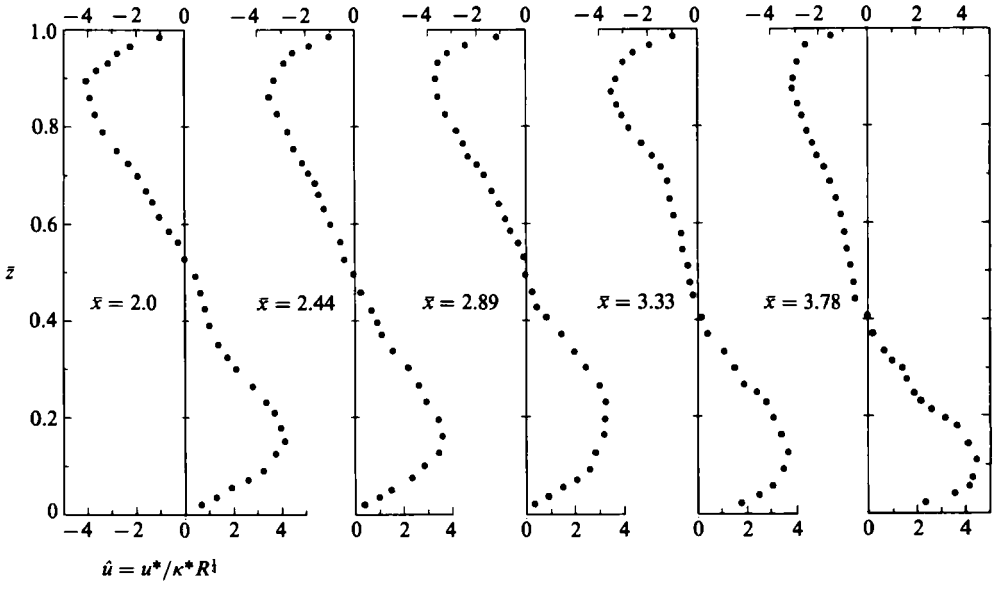

FIGURE 4. Velocity distribution; $R = 1.3 \times 10^6$, $L = 4$.

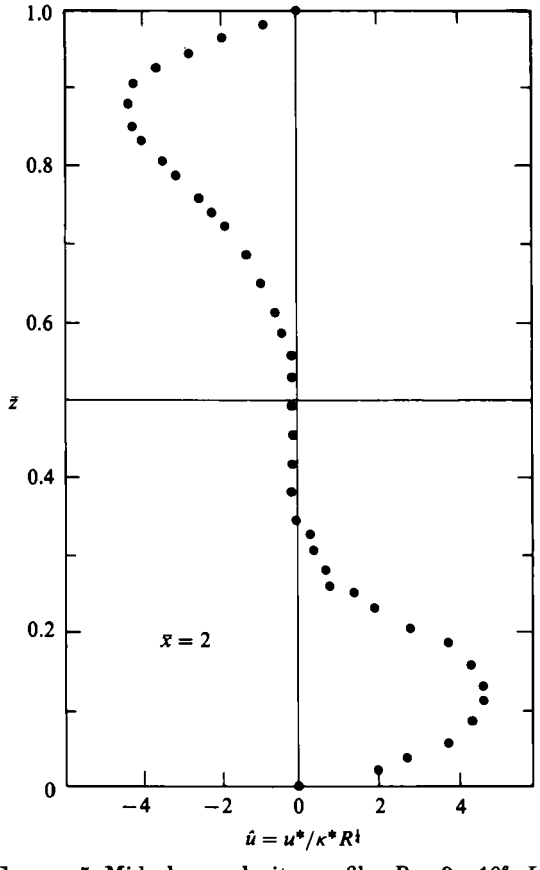

FIGURE 5. Mid-plane velocity profile; $R = 9 \times 10^6$, $L = 4$.

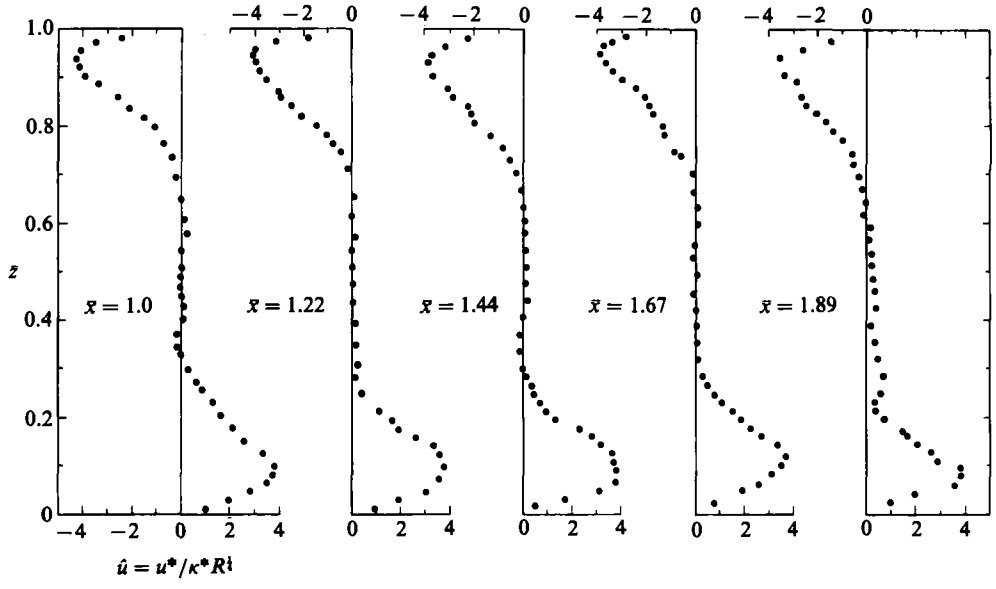

FIGURE 6. Velocity distribution; $R = 10^7$, $L = 2$.

figure 4 is different from that observed in figures 5 and 6. In figure 4 the layers adjacent to the horizontal surfaces almost fill the cavity and there is no evidence of a distinct core region. Within the experimental uncertainty, the stagnation line at the mid-plane $\bar{x} = 2.0$ (i.e. $\frac{1}{2}L$) is at the cavity half-height $\bar{z} = \frac{1}{2}$. At each location approaching the hot wall the velocity profile changes noticeably. Warm fluid being ejected from the upper portion of the vertical boundary layer causes the upper layer to become progressively thicker. A corresponding decrease in the lower layer thickness occurs as cold fluid is entrained into the boundary layer near the bottom corner of the hot wall. There is a marked increase in the maximum velocity of the cold layer at $\bar{x} = 3.78$ at which location the position of the stagnation line has dropped to $\bar{z} = 0.4$.

the aspect ratio fixed at $L = 4$. It is apparent that at the mid-plane the motion has altered significantly from that seen in figure 4: the core has become motionless and all of the mass flux is occurring in layers adjacent to the horizontal surfaces. Asymmetry is also evident in the profile, the upper warm layer being about 30% thicker than the cool layer beneath it. The development of a motionless core is unexpected and suggests the possibility of a flow reversal occurring at larger values of R if changes in the core velocity gradient continue. This conjecture has not been tested in the present work, but complementary measurements by Bejan *et al.* (1981) do show flow reversals at larger values of R and L.

A third set of traverses taken at approximately the same Rayleigh number, but with a smaller aspect ratio, are given in figure 6. These observations show that the motionless core persists throughout most of the cavity. Note that in these profiles the mid-plane data are symmetric and that again the warm layer thickness grows as $\bar{x}$ increases. By $\bar{x} = 1.89$ the departure from vertical symmetry is evident, indicating that the core flow is not parallel to the horizontal boundaries.

The stream functions $\hat{\psi}$ corresponding to particular velocity distributions given in figures 4 and 6 are shown in figures 7 and 8, respectively. Integration of the velocity profile data is carried out using a cubic spline fitting routine, which initially also

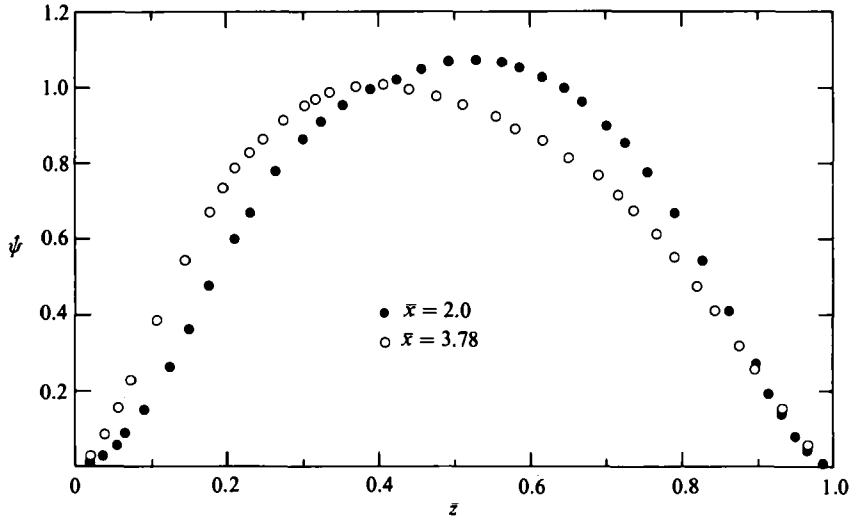

FIGURE 7. Core stream function for $R = 1.3 \times 10^6$, $L = 4$.

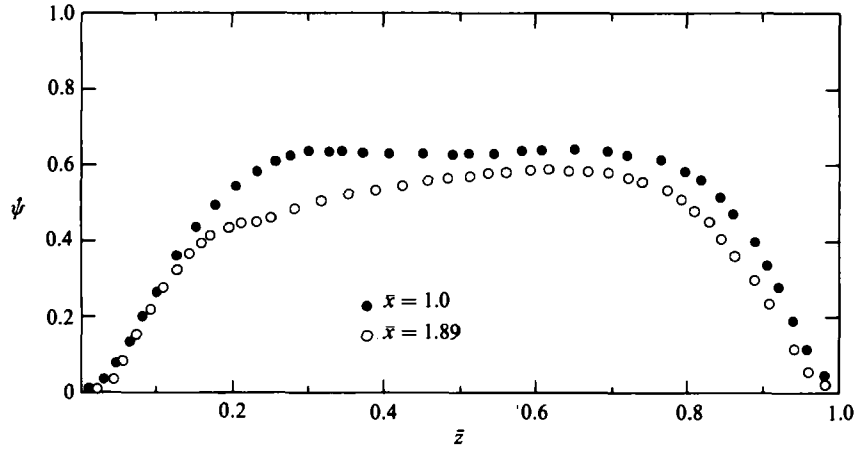

FIGURE 8. Core stream function for $R = 10^7$, $L = 2$.

locates the $\bar{u} = 0$ position to ensure that mass conservation is preserved. This procedure leads to estimated errors of approximately three per cent in the stream-function calculations. Differences between the two flow-field situations described earlier are made more apparent by the stream-function profiles. For the case where the core is filled by the layers on the horizontal surfaces the stream function has a smooth, rounded profile. In contrast, the case for which the core is motionless exhibits a flatter profile of smaller amplitude; see figure 8. Both sets of data show some x-dependence, indicating that neither situation conforms strictly to the boundary-layer regime where $\bar{\psi}$ is only a function of $\bar{z}$, (Gill 1966). All of the data recorded at the mid-plane, but not necessarily discussed here, are given in figure 9 as a function of R. Similar measurements taken earlier by Simpkins & Dudderar (1981) are also illustrated for comparison. Agreement between the two sets of measurements, taken by different methods, is good. Thus, the effect of the aspect ratio on the flow field is confirmed over the range $10^5 \leqslant R \lesssim 8 \times 10^7$, for $\sigma \geqslant 7$. It is noteworthy that only

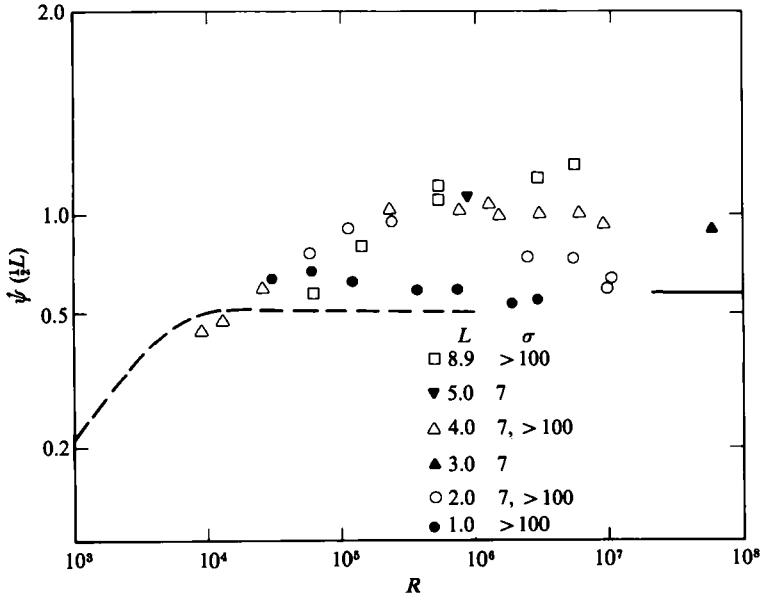

FIGURE 9. Dependence of the core stream function on aspect ratio. ——, Blythe *et al.* $R \to \infty$, $\sigma \to \infty$; ---, Vahl Davis, $L = 1$, $\sigma = 0.7$.

the data for $L = 1$ are close to the numerical solution given by Blythe *et al.* (1983) for the boundary-layer regime $R \to \infty$, $\sigma \to \infty$. Mention must be made of the result derived from the work presented in Bejan *et al.* (1981), see their figure 5 (*b*), from which a value of $\hat{\psi}(\frac{1}{2}L) \simeq 0.56$ can be deduced at $R = 1.6 \times 10^9$.

4.2. *Observations of the temperature distribution*

Temperature measurements across the cavity at various $\bar{x}$ locations are given in figure 10 and in figure 11. Across the mid-plane the temperature profiles are similar and, in dimensionless variables, the gradient at $\bar{z} = \frac{1}{2}$ is, in both cases, $(\mathrm{d}\bar{T}/\mathrm{d}\bar{z}) = 0.52$. This result is in the range 0.54 ± 0.05 suggested by earlier investigators for the laminar boundary-layer regime in tall slender cavities; e.g. see Eckert & Carlson (1961) and Elder (1965). Near the hot wall the measurements in both figures show that the constant temperature gradient in the core becomes distorted, particularly near the upper surface. In figure 10 the distortion at $\bar{x} = 3.78$ is especially pronounced: from flow visualizations it is known that this location is close to the axis of a secondary cell, see Simpkins & Chen (1985). The profile shape near the upper boundary suggests that the insulation is inadequate and that some heat loss is occurring; however, additional layers of neoprene matting made no significant difference to measurements in that vicinity. Interpolation of the data from figures 10 and 11 demonstrates that the isotherms are not parallel to the horizontal boundaries over most of the core region. This result is in accord with the velocity measurements and suggests that the flow field has not reached the boundary-layer limiting behaviour.

The data given in figure 12 represent the largest Rayleigh number measurements recorded in the present experiments. Once again there is noticeable distortion of the temperature distribution near the upper boundary which persists to the mid-plane. Within the experimental accuracy the core temperature gradient is 0.50.

Numerous interferograms have been taken of the convective flow field in the cavity by the wavefront shearing technique. Two typical steady state photographs are

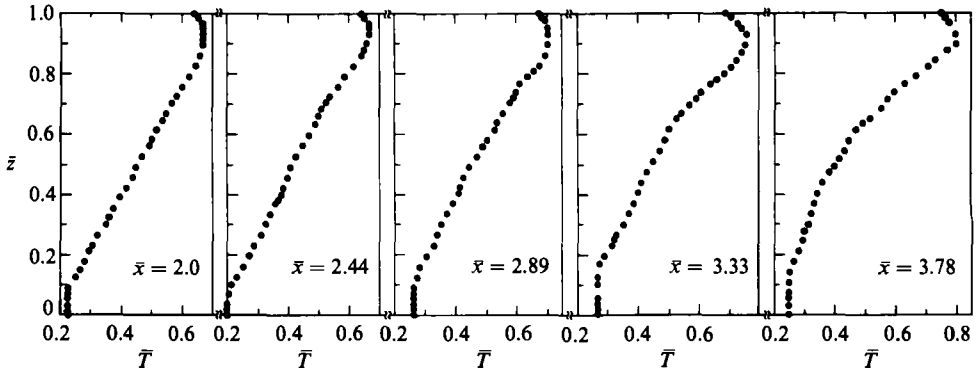

FIGURE 10. Temperature distributions; $R = 1.3 \times 10^6$, $L = 4$.

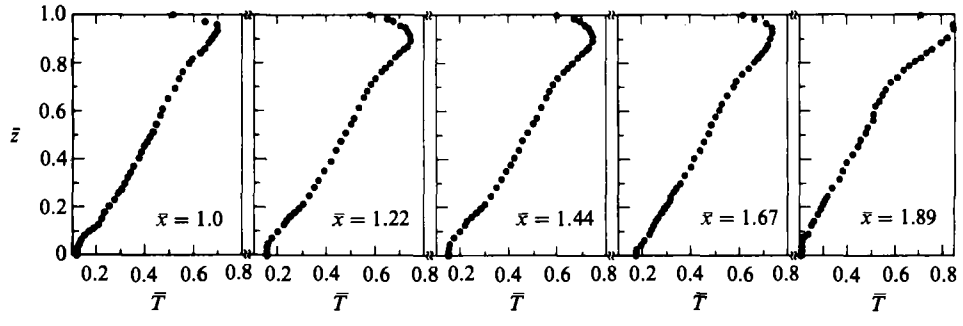

FIGURE 11. Temperature distributions; $R = 10^7$, $L = 2$.

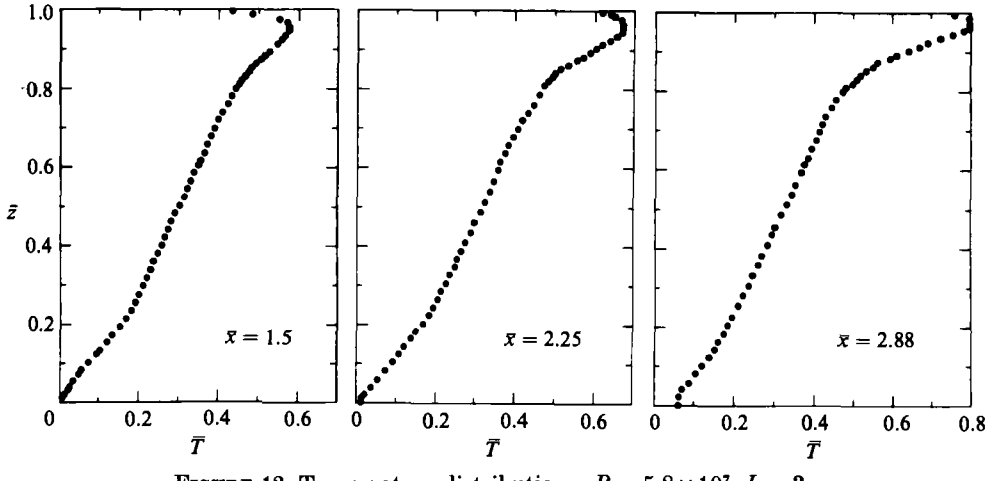

FIGURE 12. Temperature distributions; $R = 5.8 \times 10^7$, $L = 3$.

shown in figure 13. In these tests, flows with Rayleigh numbers up to 1.6×10^7 were examined for aspect ratios up to about three. The cavity length is restricted by the diameter of the collimated plane wave beam projected from the output lens, which is an air spaced doublet 112 mm in diameter, with a surface accuracy of 2λ at 632.8 nm. Within the limited range of aspect ratios that have been examined, the interferometry measurements confirm a number of findings. Most important is that,

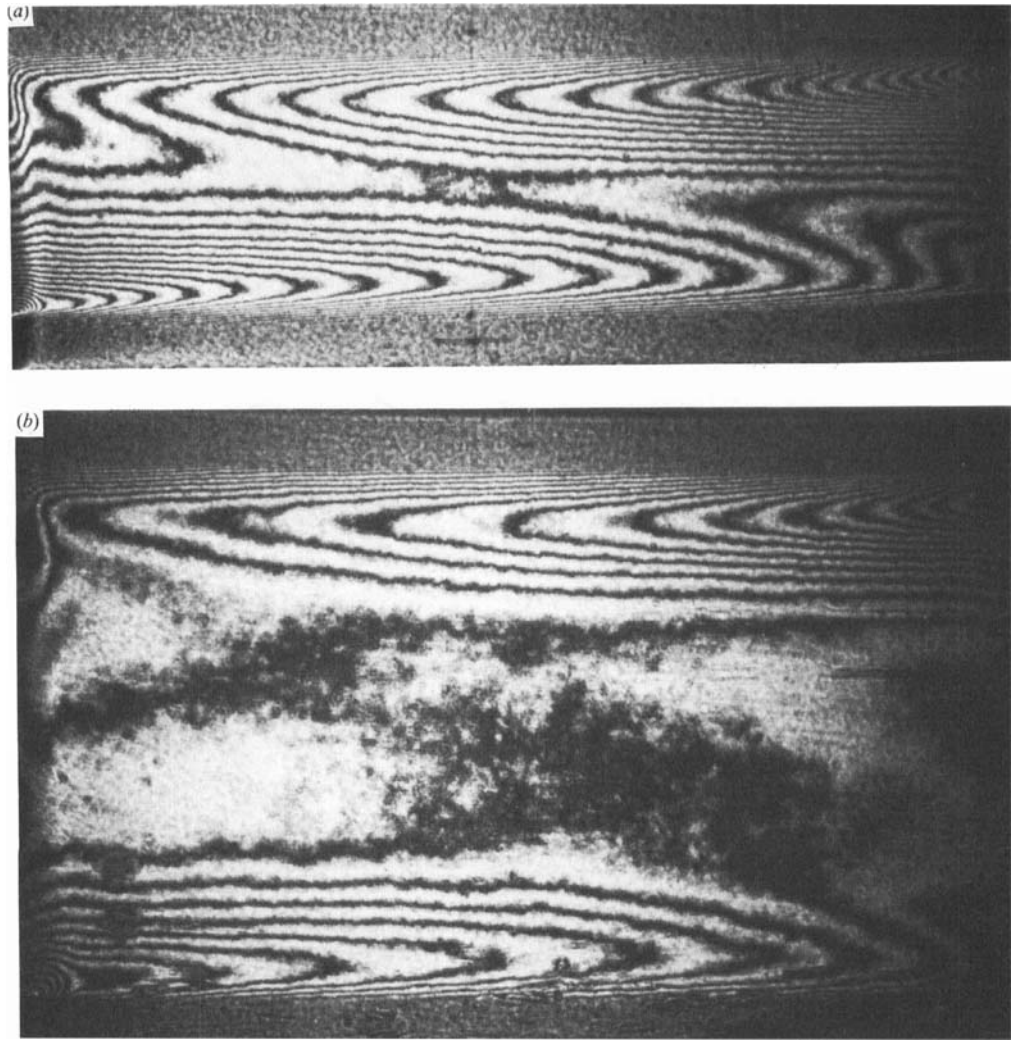

FIGURE 13. Wavefront shearing interferograms; (*a*) $R = 4.8 \times 10^6$, $L = 3.2$; (*b*) $R = 1.6 \times 10^7$, $L = 1.8$.

after steady state is reached, there is no discernible unsteadiness in the data for periods up to six hours. Secondly, the pictures shown in figure 13 reaffirm the centro-symmetric nature of the flow field. Lastly, the single fringe which spreads across the cavity mid-point, particularly in figure 13(*b*), emphasizes that the core temperature gradient is invariant.

Successive integration of the fringe orders across the cavity depth at the mid-point yields the temperature gradient profile and the temperature distribution across the cavity. These results are shown in figure 14 for the corresponding interferograms given in figure 13. Because the shearing procedure obscures the horizontal boundaries of the cavity the data is only relative, the total number of fringes in the regions adjacent to the surfaces being unknown. Nevertheless, the qualitative features given in figure 14 reveal that the two situations are quite different. The temperature and the temperature gradient profiles given in figure 14(*a*) are similar to those expected for

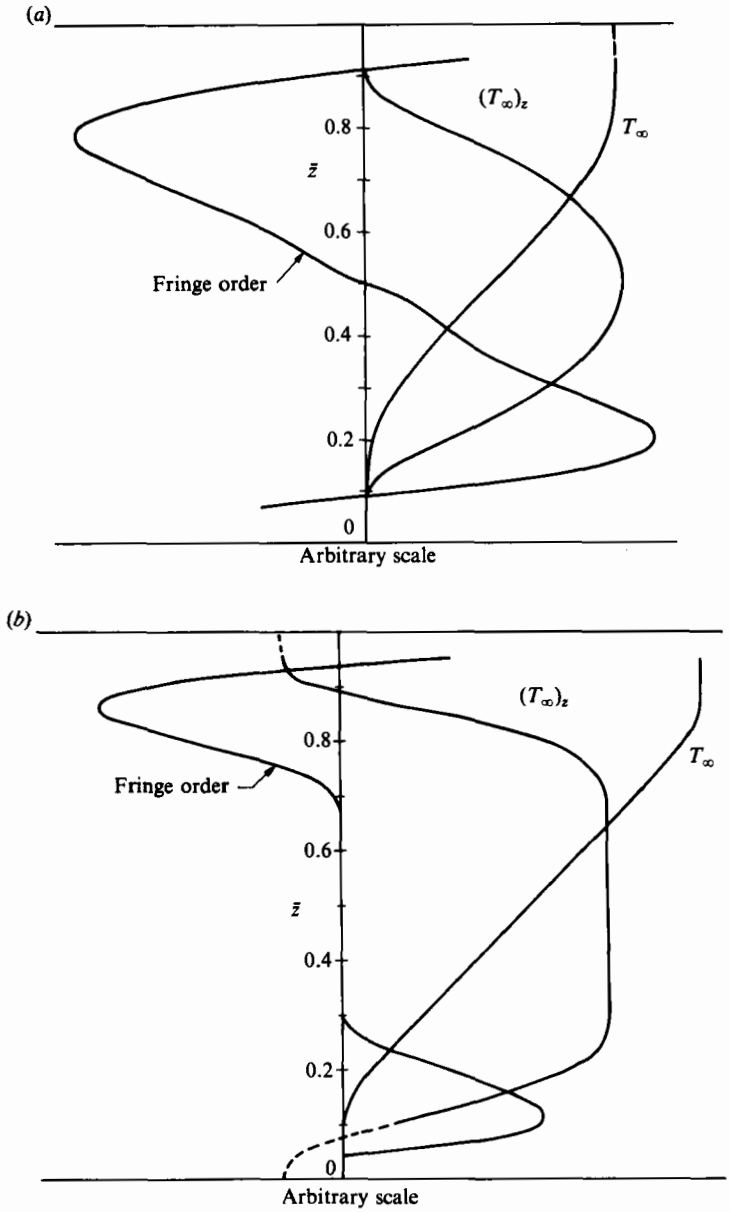

FIGURE 14. Thermal distribution profiles corresponding to figure 13. (*a*) $R = 4.8 \times 10^6$, $L = 3.2$. (*b*) $R = 1.6 \times 10^7$, $L = 1.8$.

a Hadley cell (see figure 1) suggesting that the core flow is highly diffusive. Corresponding distributions in figure 14(*b*) illustrate a situation more reminiscent of the boundary-layer regime (see figure 2). Note that diffusive effects are confined to regions near the horizontal surfaces where many fringe orders are evident, and that across the core ($\mathrm{d}T/\mathrm{d}\bar{z}$) is constant. These findings are consistent with the thermocouple probe measurements.

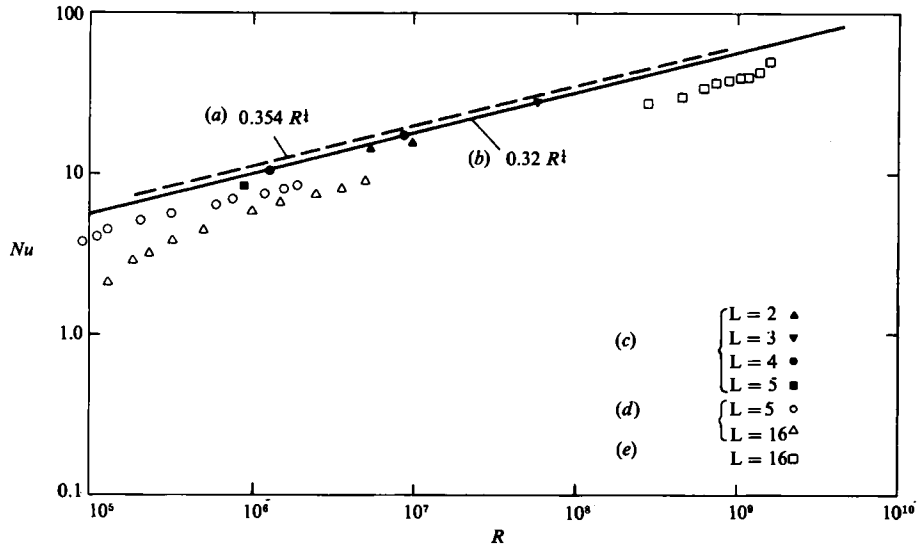

FIGURE 15. Heat transfer across the cavity. $\sigma \approx 7$ for all data. (*a*) Bejan & Tien; (*b*) Blythe *et al.* $R \gg 1$, $\sigma \to \infty$, numerical; (*c*) Present data; (*d*) Kamotani *et al.*, (*e*) Bejan *et al.*

4.3. *Heat transfer data*

Estimates of the net heat transfer per unit width have been computed in terms of the Nusselt number defined by

$$Nu = \frac{Q^*/b^*}{k^* T_w^*} = \int_0^1 \bar{u}\bar{T}\,\mathrm{d}\bar{z},$$

from the velocity distributions and temperature measurements described previously. Cubic spline fitting routines and standard integration methods were used to perform these computations. The results are presented in figure 15 together with data from other sources where water was used as the test medium in cavities with $L > 1$. All of the current data lie above that recorded by Kamotani *et al.* (1983) for $L = 5$, although the present $L = 5$ result is, within the experimental uncertainty, in agreement with those data.

A numerical solution of the vertical boundary equations by Blythe *et al.* (1983) is in good agreement with the present measurements, which are consistently below the approximate solution due to Bejan & Tien (1978). For fixed Rayleigh and Prandtl numbers the data presented in figure 15 show that the heat transfer is inversely proportional to the aspect ratio L.

A synopsis of heat transfer results, measurements of the core stream function and temperature gradient data is given in table 1. Some approximate method predictions and some numerical solutions are also included in the table. Differences in the current estimates of $NuR^{-\frac{1}{4}}$ are within the anticipated numerical errors of the computations mentioned above. Most of this uncertainty is caused by adjustments made in the $u(z)$ profile to satisfy continuity.

Examination of table 1 suggests that the core temperature gradient and the heat transfer are not very sensitive measures of variations in R, L and σ. In contrast, the core stream function is seen to be very sensitive to changes in R and L and, to a lesser extent, to variations in σ. Results given in table 1 also show that although the approximate models give good agreement with the characteristic values of the heat

	$\hat{\psi}_\infty(\frac{1}{2})$	$\hat{T}'_\infty(\frac{1}{2})$	$NuR^{-\frac{1}{4}}$	$R\times10^{-6}$	L	σ	Remarks
Bejan & Tien (1978)	—	1.0	0.354	∞	—	—	A
Bejan *et al.* (1981)	—	0.46*	0.22*	1220	16	7.1	X
Bejan *et al.* (1981)	0.56*	0.48*	0.25*	1590	16	7.1	X
Blythe *et al.* (1983)	0.59	0.52	0.32	∞	—	∞	N
Blythe & Simpkins (1977)	0.66	0.57	0.30	∞	—	∞	A
Elder (1965)	—	0.52*	—	77	0.25	100	X
Gill (1966)	0.76	0.41	—	∞	—	∞	A
Quon (1972)	0.57	0.52*	0.27	0.8	1	7.1	N
Shiralkar *et al.* (1981)	—	0.80*	0.27	10	5	1	A
Simpkins & Dudderar (1981)	0.75	—	—	2.5	2	10^3	X
Simpkins & Dudderar (1981)	1.0	—	—	1.5	4	10^3	X
Simpkins & Dudderar (1981)	1.55	—	—	2.9	9	10^3	X
Tichy & Gadgil (1982)	—	0.75	0.27	10	5	1	A
Vahl Davis & Jones (1982)	0.51	—	0.22	10^{-2}	1	0.7	N
Vahl Davis & Jones (1982)	0.52	—	0.28	1.0	1	0.7	N
Present	0.64	0.51	0.31	10.3	2	7.1	X
Present	0.94	0.54	0.29	9.1	4	7.1	X
Present	1.07	0.53	0.31	1.3	4	7.1	X

TABLE 1. Comparison of the characteristic flow field properties from experimental (X), numerical (N), and approximate (A) data. Starred values are only estimates.

transfer across the cavity, notable differences occur in the magnitude of the core temperature gradient necessary to achieve this. It should be noted here that the authors have stressed that their predictions of Nu are very sensitive to the constant of integration found from their various matching criteria.

5. Conclusions

The non-intrusive velocity and interferometry measurements, together with the locally recorded temperature distributions, reveal the following characteristic properties of the convection in a rectangular cavity with $\sigma \approx 7$. (i) For $R > O(10^5)$ the core stream function is dependent on the aspect ratio, confirming the visual measurements by Simpkins & Dudderar (1981). (ii) Away from the vertical endwalls when $R \sim 10^6$, $L \sim 3$, the flow comprises a slow moving core between thick layers adjacent to the horizontal surfaces. As R increases the LDV measurements reveal that the core horizontal velocity gradient decreases and the mass transported via the horizontal layers increases. This observation, which is confirmed by the interferometry data, suggests the possibility of a flow reversal evolving in the core at larger values of R. (iii) Measurements of the vertical temperature gradient are in good agreement with numerical solutions of the vertical boundary-layer equations. It has been noted, however, that this measurement is not a sensitive gauge of the flow field to changes in R and L. The observations suggest that the core is stably stratified with a characteristic temperature gradient of 0.53 ± 0.03 for $10^6 \leqslant R \leqslant 10^8$ and $L > 1$. (iv) Nusselt number computations based on the core velocity and core temperature measurements are in good agreement with the numerical solution of Blythe *et al.* (1983) and, to a lesser degree, with the approximation due to Bejan & Tien (1978).

The authors thank Professor P. A. Blythe of Lehigh University for helpful discussions and Dr R. Meynart of Brussels University for drawing their attention to the shearing interferometry technique. This work was partially supported by the National Science Foundation under Grant No. MEA-8115333.

REFERENCES

BATCHELOR, G. 1954 *Q. Appl. Maths* **12**, 209.

BEJAN, A. & TIEN, C. L. 1978 *Trans ASME J. Heat Transfer* **100**, 641.

BEJAN, A., AL-HOMOUD, A. A. & IMBERGER, J. 1981 *J. Fluid Mech.* **109**, 283.

BLYTHE, P. A. & SIMPKINS, P. G. 1977 *Physico-chemical Hydrodynamics* **2**, 511.

BLYTHE, P. A., DANIELS, P. G. & SIMPKINS, P. G. 1983 *Proc. R. Soc. Lond.* A **387**, 367.

BRIGGS, D. G. & JONES, D. N. 1982 unpublished, *ASME Paper* 82-WA/HT-64.

BRYNGDAHL, O. 1965 *Progress in Optics* **4**, 37.

CATTON, I. 1978 *Proc. 6th Int. Heat Trans. Conf.* **6**, 13.

CORMACK, D. E., LEAL, L. G. & IMBERGER, J. 1974 *J. Fluid Mech.* **65**, 209.

ECKERT, E. R. G. & CARLSON, W. O. 1961 *Intl J. Heat Mass Transfer* **2**, 106.

ELDER, J. W. 1965 *J. Fluid Mech.* **23**, 77.

GILL, A. E. 1966 *J. Fluid Mech.* **26**, 515.

HADLEY, G. 1735 *Phil. Trans. R. Soc. Lond.* **29**, 58.

HART, J. E. 1972 *J. Atmos. Sci.* **29**, 687.

HART, J. E. 1983*a* *J. Fluid Mech.* **132**, 271.

HART, J. E. 1983*b* *Intl J. Heat Mass Transfer* **26**, 1069.

IMBERGER, J. 1974 *J. Fluid Mech.* **65**, 247.

KAMOTANI, Y., WANG, L. W. & OSTRACH, S. 1983 *AIAAJ.* **21**, 290.

KIRDYASHKIN, A. G. 1984 *Intl J. Heat Mass Transfer* **27**, 587.

MERZKIRCH, W. 1974 *Flow Visualization*, ch. 3, pp. 129–31. Academic.

OSTRACH, S. 1972 *Adv. Heat Transfer* **8**, 161.

QUON, C. 1972 *Phys. Fluids* **15**, 12.

QUON, C. 1977 *Trans ASME J. Heat Transfer* **99**, 341.

SCHIROKY, G. H. & ROSENBERGER, F. 1984 *Intl J. Heat Mass Transfer* **27**, 587.

SHIRALKAR, G., GADGIL, A. & TIEN, C. L. 1981 *Intl J. Heat Mass Transfer* **24**, 1621.

SIMPKINS, P. G. & CHEN, K. S. 1985 *Natural Convection: Fundamentals and Applications* (ed. Kakaç, S., Aung, W. & Viskanta, R.), p. 1010. Hemisphere.

SIMPKINS, P. G. & DUDDERAR, T. D. 1981 *J. Fluid Mech.* **110**, 433.

SINGH, K. R. & COWLING, T. G. 1963 *Q. J. Mech. Appl. Maths* **16**, 17.

SQUIRE, H. B. 1953 *Modern Developments in Fluid Dynamics, High Speed Flow* (ed. Howarth, L.), ch. 14. Clarendon.

TICHY, J. & GADGIL, A. 1982 *Trans ASME J. Heat Transfer* **104**, 103.

VAHL DAVIS, G. DE & JONES, I. P. 1982 *Univ. New South Wales (Kensington, Aust. 2033) Rept.* 1982/FMT/3.

WILMSHURST, T. H. & RIZZO, J. E. 1974 *J. Phys. E: Sci. Instrum.* **7**, 924.